Finite element simulation of piezoelectric vibrator gyroscopes

Yukio Kagawa
Okayama University

Takao Tsuchiya
Okayama University

Toshikazu Kawashima
Okayama University

Finite Element Simulation of Piezoelectric Vibrator Gyroscopes

Yukio Kagawa, *Fellow, IEEE,* Takao Tsuchiya, and Toshikazu Kawashima

***Abstract*— A finite element approach to the simulation of piezoelectric vibrator gyroscopes is presented for characteristic prediction. The formulation is given including the effect of Coriolis force due to rotation for a piezoelectric thin plate, which is considered to be two-dimensional in plane vibration. For numerical examples, the gyroscopes of a thin square plate, and a cross-bar and a ring built in the plate are considered, which pave the way for the development of the gyroscopes of monolithic configuration. The effect of the rotation on the modal shapes, the resonant frequencies, and the transmission characteristics are discussed demonstrating the sensing capability against the rotation.**

NOMENCLATURE

$\boldsymbol{S}$ Strain vector $\{S_1\ S_2\ S_6\} = \{u_{x,x}\ u_{y,y}\ u_{x,y} + u_{y,x}\}$, where S_1 and S_2 are strains in the x and y direction, respectively, and S_6 is a shear strain in the x–y plane.

$\boldsymbol{T}$ Strain vector $\{T_1\ T_2\ T_6\}$, where T_1 and T_2 are stresses in the x and y direction, respectively, and T_6 is the shear stress in the x–y plane.

$\boldsymbol{s}^E$ Elastic constant tensor ($E = 0$).

$\boldsymbol{d}$ Piezoelectric constant tensor $\{d_{31}\ d_{32}\ d_{36}\}$.

$\boldsymbol{\theta}$ Gyro matrix

$$\begin{bmatrix} 0 & 1 \\ -1 & 0 \end{bmatrix}.$$

$\boldsymbol{\xi}_e$ Nodal displacement vector of elements e

$$\{u_{x1}\ u_{x2}\ u_{x3}\ u_{x4}\ u_{x5}\ u_{x6}\ u_{y1}\ u_{y2}\ u_{y3}\ u_{y4}\ u_{y5}\ u_{y6}\}.$$

$\boldsymbol{\phi}_e$ Nodal potential vector of elements e

$$\{\phi_1\ \ \phi_2\ \ \phi_3\ \ \phi_4\ \ \phi_5\ \ \phi_6\}.$$

$\boldsymbol{N}$ Second-order interpolation function vector

$$[A]^* \{\zeta_1^2\ \ \zeta_2^2\ \ \zeta_3^2\ \ \zeta_2\zeta_3\ \ \zeta_3\zeta_1\ \ \zeta_1\zeta_2\}$$

where

$$[A] = \begin{bmatrix} 1 & 0 & 0 & 0 & 0 & 0 \\ 0 & 1 & 0 & 0 & 0 & 0 \\ 0 & 0 & 1 & 0 & 0 & 0 \\ 0 & -1 & -1 & 4 & 0 & 0 \\ -1 & 0 & -1 & 0 & 4 & 0 \\ -1 & -1 & 0 & 0 & 0 & 4 \end{bmatrix}.$$

$\boldsymbol{n}$ Differential vector of interpolation function

$$\{\zeta_1\ \ \zeta_2\ \ \zeta_3\}.$$

ζ_i Area coordinates

$$\zeta_i = \frac{a_i + b_i x + c_i y}{2\Delta_e}$$

where

$$a_i = x_j y_m - x_m y_j$$
$$b_i = y_j - y_m$$
$$c_i = x_m - x_j$$

(i, j, and m permute in the order of node 1, 2, and 3, and x_i and y_i are the coordinate values corresponding to node i).

$\boldsymbol{B}_e$ Differential coefficient matrix for the x direction

$$\begin{bmatrix} 3b_1 & -b_2 & -b_3 & 0 & 4b_3 & 4b_2 \\ -b_1 & 3b_2 & -b_3 & 4b_3 & 0 & 4b_1 \\ -b_1 & -b_2 & 3b_3 & 4b_2 & 4b_1 & 0 \end{bmatrix}.$$

$\boldsymbol{C}_e$ Differential coefficient matrix for the y direction, in which b_i in $\boldsymbol{B}_e$ is replaced by c_i.

$\boldsymbol{I}_n$ Unit matrix of $n \times n$.

$\boldsymbol{\Theta}$ Matrix associated with rotation

$$\begin{bmatrix} \mathbf{0} & \boldsymbol{I}_6 \\ -\boldsymbol{I}_6 & \mathbf{0} \end{bmatrix}.$$

f_{LB} Natural frequency of longitudinal vibration of a bar with length a [$= 1/(2a\sqrt{s_{11}^E \rho})$].

ω_{LB} $2\pi f_{LB}$.

$\overline{f}$ Normalized frequency ($= f/f_{LB}$).

$\overline{\Omega}$ Normalized angular velocity ($= \Omega/2\pi f_{LB}$).

Manuscript received June 19, 1995; revised February 14, 1996. This work was supported in part by Grant in Aid for Scientific Research (C), 05650236, the Ministry of Education, Science, and Culture. The contents of this paper were presented in part at the Technical Meeting of The Institute of Electronics, Information, and Communication Engineers, Japan [12].

The authors are with the Department of Electrical and Electronic Engineering, Faculty of Engineering, Okayama University, 3-1-1 Tsushima-naka, Okayama 700, Japan (e-mail: kagawa@calc.elec.okayama-u.ac.jp).

Publisher Item Identifier S 0885-3010(96)04951-9.

I. Introduction

VIBRATOR gyroscopes are used as the sensors for detecting angle and angular velocity like any other gyroscope. The piezoelectric vibrator gyroscopes provide piezoelectric transducers for excitation and detection. Their operation is based on the principle that a secondary vibration is generated in the direction lateral to the original vibration of the vibrator in rotation due to Coriolis force. The angular velocity of the rotation can thus be sensed by measuring the amplitude of this lateral vibration induced or transmitted from the exciting vibration [1]. For the analysis of the operational characteristic of the piezoelectric vibrator gyroscopes, both equivalent circuit and analytical approaches have been used which are limited to the gyroscopes of simple configuration [2], [3]. They are difficult to apply to the gyroscopes of general shape for developing the best possible configuration and temperature characteristics. Numerical approaches should be sought for this purpose. Piezoelectric materials involve the energy exchange between the mechanical and electrical energy, for which the finite element method can effectively be utilized as it is based on the energy principle. Since its first introduction to the analysis of piezoelectric vibrators [4], it has extensively been used for the design of vibrators, sensors, and transducers, for which is now well established [5], [6]. The application of the finite element method to the analysis of rotational sensors was recently tried but no successful example was given [7].

In the present paper, the finite element formulation for a piezoelectric vibrator in rotation is developed including effects both of piezoelectricity and Coriolis force. A thin plate in plane vibration rotating in that plane is considered, for which the development of the monolithic type being fabricated with a lithographic process is intended.

For numerical examples, the piezoelectric vibrator gyroscopes consisting of a thin square plate, a cross-bar, and a ring built in the plate are considered. The effect of the rotation on the modal shapes and the resonant frequencies, and the transmission characteristics are discussed demonstrating the sensing capability against the rotation.

II. Vibratory System in Rotation

As shown in Fig. 1, a thin piezoelectric plate vibrates in its x–y plane with constant angular frequency ω, which also rotates around the z axis with constant angular velocity Ω. Equations of motion for a particle ρ in steady-state motion are given as follows:

$$\left.\begin{aligned} f_x &= F_x + \rho\omega^2 u_x + j2\rho\Omega\omega u_y + \rho\Omega^2 x \\ f_y &= F_y + \rho\omega^2 u_y - j2\rho\Omega\omega u_x + \rho\Omega^2 y \end{aligned}\right\} \quad (1)$$

where f stands for total force acting on the particle, ρ is mass of the particle, F is external force, u is particle displacement, and x, y are the coordinates of the particle. The second terms on the right-hand side of (1) are the inertia forces due to the vibration, the third terms are the Coriolis forces, and the fourth terms are the centrifugal forces. When the plate rotates around the z axis, the Coriolis force is generated in the direction lateral to the displacement of the vibration. Coriolis forces and centrifugal forces both act in the x–y plane. If $\omega \gg \Omega$, the effects of the centrifugal forces or the last terms could be ignored.

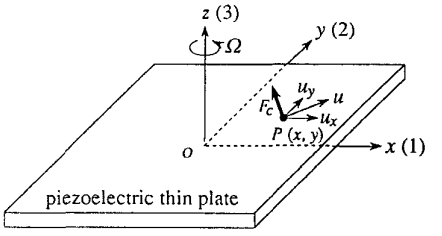

Fig. 1. Coordinates and Coriolis force in rotation.

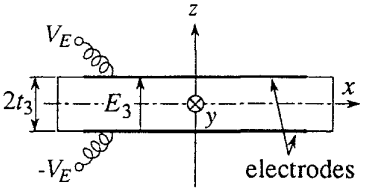

Fig. 2. Piezoelectric thin plate in plane motion (cross-sectional view).

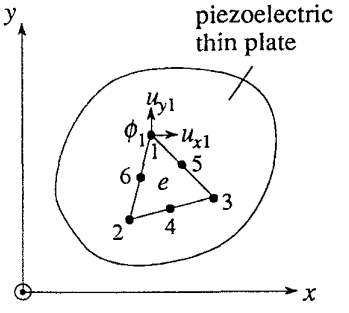

Fig. 3. Piezoelectric field and triangular element (second-order polynominal interpolation function, plain view).

III. Finite Element Formulation for Piezoelectric Vibratory System in Rotation

Finite element analysis is a method of transforming a continuum system to its equivalent discretized system in which the system is divided into elements. Here, a thin piezoelectric plate is shown in Fig. 2, in which the plate is divided into triangular elements with the second-order polynomial function interpolated as shown in Fig. 3. Pairs of partial electrodes are placed on both surfaces of the piezoelectric thin plate. As the thin plate vibrates in its x–y plane, it is assumed that the strain is independent of thickness or z direction, and the electric field is parallel to the z direction and constant. The piezoelectric constitutive expressions of d-type in the present case are

$$\left.\begin{aligned} \boldsymbol{S} &= \boldsymbol{s}^E\boldsymbol{T} + \boldsymbol{d}E_3 \\ D_3 &= \boldsymbol{d}^*\boldsymbol{T} + \varepsilon_{33}^T E_3 \end{aligned}\right\} \quad (2)$$

where $\boldsymbol{s}^E$ is the elastic modulus tensor ($E_3 = 0$), $\boldsymbol{T}$ is the stress vector, $\boldsymbol{d}$ is the piezoelectric constant vector, E_3, D_3 is the electric field and electric displacement in the z direction, ε_{33}^T is the dielectric constant in the z direction ($\boldsymbol{T} = \boldsymbol{0}$), and $(\,)^*$ is the transposition of the matrix or vector.

It is assumed that the direction of polarization is parallel to the z direction. (The concrete definition for the components is given in the Nomenclature.)

Suppose that the plate is divided into triangular elements. Within an element e, displacement vector $\boldsymbol{u}_e = \{u_x(x, y), u_y(x, y)\}$ and the potential $\varphi_e = \varphi(x, y)$ are, respectively, defined and expressed in terms of the linear combination of nodal displacement vector $\boldsymbol{\xi}_e$ and nodal potential vector $\boldsymbol{\phi}_e$ defined at the nodal coordinates $(x_i, y_i)\,(i = 1 - 6)$ as

$$\boldsymbol{u}_e = \begin{bmatrix} \boldsymbol{N}^* & \boldsymbol{0} \\ \boldsymbol{0} & \boldsymbol{N}^* \end{bmatrix} \boldsymbol{\xi}_e \tag{3}$$

$$\varphi_e = \boldsymbol{N}^* \boldsymbol{\phi}_e \tag{4}$$

where $\boldsymbol{\xi}_e$ is the nodal displacement, $\boldsymbol{\phi}_e$ is the nodal potential vector, and $\boldsymbol{N}$ is the interpolation function vector.

The strain vector $\boldsymbol{S}_e$, which is the derivative of the displacement with respect to the coordinates, is expressed as

$$\boldsymbol{S}_e = \frac{1}{2\Delta_e} \begin{bmatrix} \boldsymbol{n}^* & \boldsymbol{0} & \boldsymbol{0} \\ \boldsymbol{0} & \boldsymbol{n}^* & \boldsymbol{0} \\ \boldsymbol{0} & \boldsymbol{0} & \boldsymbol{n}^* \end{bmatrix} \begin{bmatrix} \boldsymbol{B}_e & \boldsymbol{0} \\ \boldsymbol{0} & \boldsymbol{C}_e \\ \boldsymbol{C}_e & \boldsymbol{B}_e \end{bmatrix} \boldsymbol{\xi}_e \tag{5}$$

where Δ_e is the area of the triangular element, $\boldsymbol{n}$ is the vector associated with the derivative of the interpolation function, and $\boldsymbol{B}_e$, $\boldsymbol{C}_e$ are the coefficient matrices associated with the derivative of the interpolation function with respect to the x or y direction. The z directional electric field E_{3e} in the element is expressed with the nodal potential vector $\boldsymbol{\phi}_e$ as

$$\begin{aligned} E_{3e} &= -\frac{2\varphi_e}{2t_3} \\ &= -\frac{1}{t_3} \boldsymbol{N}^* \boldsymbol{\phi}_e \end{aligned} \tag{6}$$

for the piezoelectric plate of thickness $2t_3$.

The energy functional for a piezoelectric vibrator consists of strain energy, kinetic energy, electrostatic energy, and work done by external forces. In the finite element method, the energy functional is minimized applying the variational principle. However, when the system dissipates or rotates, the energy functional becomes complex. Here, an adjoint system is introduced to establish that the functional is real [8], in which case the physical meaning of minimization is much clearer. Strain energy U_e, electrostatic energy H_e, and kinetic energy T_e are thus defined for the element e as follows:

$$\begin{aligned} U_e &= \tfrac{1}{8} \iiint_e (\boldsymbol{S}_e^* \tilde{\boldsymbol{T}}_e + \tilde{\boldsymbol{S}}_e^* \underline{\boldsymbol{T}}_e + \underline{\boldsymbol{S}}_e^* \tilde{\boldsymbol{T}}_e + \tilde{\underline{\boldsymbol{S}}}_e^* \boldsymbol{T}_e)\, dx\, dy\, dz \\ &= \frac{t_3}{2} (\boldsymbol{\xi}_e^* \boldsymbol{K}_e \tilde{\underline{\boldsymbol{\xi}}}_e + \tilde{\boldsymbol{\xi}}_e^* \boldsymbol{K}_e \underline{\boldsymbol{\xi}}_e) \\ &\quad + \frac{t_3}{4} (\boldsymbol{\xi}_e^* \boldsymbol{P}_e \tilde{\underline{\boldsymbol{\phi}}}_e + \tilde{\boldsymbol{\xi}}_e^* \boldsymbol{P}_e \underline{\boldsymbol{\phi}}_e + \underline{\boldsymbol{\xi}}_e^* \boldsymbol{P}_e \tilde{\boldsymbol{\phi}}_e + \tilde{\underline{\boldsymbol{\xi}}}_e^* \boldsymbol{P}_e \boldsymbol{\phi}_e) \end{aligned} \tag{7}$$

$$\begin{aligned} H_e &= \tfrac{1}{8} \iiint_e (\boldsymbol{E}_e^* \tilde{\underline{\boldsymbol{D}}}_e + \tilde{\boldsymbol{E}}_e^* \underline{\boldsymbol{D}}_e + \underline{\boldsymbol{E}}_e^* \tilde{\boldsymbol{D}}_e + \tilde{\underline{\boldsymbol{E}}}_e^* \boldsymbol{D}_e)\, dx\, dy\, dz \\ &= -\frac{t_3}{4} (\boldsymbol{\phi}_e^* \boldsymbol{P}_e \tilde{\underline{\boldsymbol{\xi}}}_e + \tilde{\boldsymbol{\phi}}_e^* \boldsymbol{P}_e \underline{\boldsymbol{\xi}}_e + \underline{\boldsymbol{\phi}}_e^* \boldsymbol{P}_e \tilde{\boldsymbol{\xi}}_e + \tilde{\underline{\boldsymbol{\phi}}}_e^* \boldsymbol{P}_e \boldsymbol{\xi}_e) \\ &\quad + \frac{t_3}{2} (\boldsymbol{\phi}_e^* \boldsymbol{G}_e \tilde{\underline{\boldsymbol{\phi}}}_e + \tilde{\boldsymbol{\phi}}_e^* \boldsymbol{G}_e \underline{\boldsymbol{\phi}}_e) \end{aligned} \tag{8}$$

$$\begin{aligned} T_e &= \tfrac{1}{8} \iiint_e (\boldsymbol{u}_e^* \tilde{\underline{\boldsymbol{f}}}_e + \tilde{\boldsymbol{u}}_e^* \underline{\boldsymbol{f}}_e + \underline{\boldsymbol{u}}_e^* \tilde{\boldsymbol{f}}_e + \tilde{\underline{\boldsymbol{u}}}_e^* \boldsymbol{f}_e)\, dx\, dy\, dz \\ &= \frac{t_3}{2} \omega^2 \left\{ \tilde{\underline{\boldsymbol{\xi}}}_e^* \left(\boldsymbol{I}_{12} + j2 \frac{\Omega}{\omega} \boldsymbol{\Theta} \right) \boldsymbol{M}_e \boldsymbol{\xi}_e \right. \\ &\quad \left. + \tilde{\boldsymbol{\xi}}_e^* \left(\boldsymbol{I}_{12} + j2 \frac{\Omega}{\omega} \boldsymbol{\Theta} \right) \boldsymbol{M}_e \underline{\boldsymbol{\xi}}_e \right\} \end{aligned} \tag{9}$$

where $\boldsymbol{K}_e$ is the stiffness matrix, $\boldsymbol{P}_e$ is the electromechanical coupling matrix, $\boldsymbol{G}_e$ is the electrostatic matrix, $\boldsymbol{\Theta}$ is the matrix of rotation, $\boldsymbol{M}_e$ is the mass matrix, and $\boldsymbol{I}_n$ is the $n \times n$ unit matrix. $(\underline{\ })$ refers to the adjoint system and $(\tilde{\ })$ to the complex conjugate. No mechanical work externally applied is considered. As the system is mechanically and electrically damped due to structural and dielectric loss, both mechanical (R_{me}) and electrical (R_{ge}) energy losses must be included, which are given as follows:

$$\begin{aligned} R_{me} &= \frac{j}{8} \frac{1}{Q_{me}} \iiint_e (-\boldsymbol{S}_e^* \tilde{\boldsymbol{T}}_e^E + \tilde{\boldsymbol{S}}_e^* \underline{\boldsymbol{T}}_e^E \\ &\quad + \underline{\boldsymbol{S}}_e^* \tilde{\boldsymbol{T}}_e^E - \tilde{\underline{\boldsymbol{S}}}_e^* \boldsymbol{T}_e^E)\, dx\, dy\, dz \\ &= j \frac{t_3}{2} \frac{1}{Q_{me}} (-\boldsymbol{\xi}_e^* \boldsymbol{K}_e \tilde{\underline{\boldsymbol{\xi}}}_e + \tilde{\boldsymbol{\xi}}_e^* \boldsymbol{K}_e \underline{\boldsymbol{\xi}}_e) \end{aligned} \tag{10}$$

$$\begin{aligned} R_{ge} &= \frac{j}{8} \tan \delta_e \iiint_e (-\boldsymbol{E}_e^* \tilde{\underline{\boldsymbol{D}}}_e^T + \tilde{\boldsymbol{E}}_e^* \underline{\boldsymbol{D}}_e^T \\ &\quad + \underline{\boldsymbol{E}}_e^* \tilde{\boldsymbol{D}}_e^T - \tilde{\underline{\boldsymbol{E}}}_e^* \boldsymbol{D}_e^T)\, dx\, dy\, dz \\ &= j \frac{t_3}{2} \tan \delta_e (-\boldsymbol{\phi}_e^* \boldsymbol{G}_e \tilde{\underline{\boldsymbol{\phi}}}_e + \tilde{\boldsymbol{\phi}}_e^* \boldsymbol{G}_e \underline{\boldsymbol{\phi}}_e) \end{aligned} \tag{11}$$

where Q_{me} is the mechanical quality factor of the material, $\boldsymbol{T}^E$ is the stress vector $(E_3 = 0)$, $\tan \delta_e$ is the tangent of dielectric loss factor, and $\boldsymbol{D}^T$ is the dielectric flux density $(\boldsymbol{T} = \boldsymbol{0})$.

The dielectric loss is taken into account only over the region where the electrodes are provided. External work W is only electrically made through the electrodes A_p due to the charges applied, which is given as follows:

$$\begin{aligned} W &= \frac{2t_3}{4} \iint_{Ap} (\varphi \tilde{\underline{\hat{D}}}_n + \tilde{\varphi} \underline{\hat{D}}_n + \underline{\varphi} \tilde{\hat{D}}_n + \tilde{\underline{\varphi}} \hat{D}_n)\, dA \\ &= \frac{t_3}{2} (\boldsymbol{\phi}^* \tilde{\underline{\hat{\boldsymbol{q}}}} + \tilde{\boldsymbol{\phi}}^* \underline{\hat{\boldsymbol{q}}} + \underline{\boldsymbol{\phi}}^* \tilde{\hat{\boldsymbol{q}}} + \tilde{\underline{\boldsymbol{\phi}}}^* \hat{\boldsymbol{q}}) \end{aligned} \tag{12}$$

where D_n is the electric (displacement) flux density normal to the boundary, and $\boldsymbol{q}$ is the nodal charge vector corresponding to the electrodes. $(\hat{\ })$ refers to known value. Lagrangian $\mathcal{L}$ for the whole system is thus given with the compatibility implied on the connecting nodes as follows:

$$\begin{aligned} \mathcal{L} &= \sum_e (U_e - H_e - T_e - R_{me} - R_{ge}) - W \\ &= \frac{t_3}{2} \tilde{\underline{\boldsymbol{\xi}}}^* \left\{ \left(1 + j \frac{1}{Q_m} \right) \boldsymbol{K} - \omega^2 \left(\boldsymbol{I} + j2 \frac{\Omega}{\omega} \boldsymbol{\Theta} \right) \boldsymbol{M} \right\} \boldsymbol{\xi} \\ &\quad + \frac{t_3}{2} \tilde{\boldsymbol{\xi}}^* \left\{ \left(1 - j \frac{1}{Q_m} \right) \boldsymbol{K} - \omega^2 \left(\boldsymbol{I} + j2 \frac{\Omega}{\omega} \boldsymbol{\Theta} \right) \boldsymbol{M} \right\} \underline{\boldsymbol{\xi}} \\ &\quad + \frac{t_3}{2} (\boldsymbol{\xi}^* \boldsymbol{P} \tilde{\underline{\boldsymbol{\phi}}} + \tilde{\boldsymbol{\xi}}^* \boldsymbol{P} \underline{\boldsymbol{\phi}} + \underline{\boldsymbol{\xi}}^* \boldsymbol{P} \tilde{\boldsymbol{\phi}} + \tilde{\underline{\boldsymbol{\xi}}}^* \boldsymbol{P} \boldsymbol{\phi}) \\ &\quad - \frac{t_3}{2} \{ (1 - j \tan \delta) \boldsymbol{\phi}^* \boldsymbol{G} \tilde{\underline{\boldsymbol{\phi}}} + (1 + j \tan \delta) \tilde{\boldsymbol{\phi}}^* \boldsymbol{G} \underline{\boldsymbol{\phi}} \} \\ &\quad - \frac{t_3}{2} (\boldsymbol{\phi}^* \tilde{\underline{\hat{\boldsymbol{q}}}} + \tilde{\boldsymbol{\phi}}^* \underline{\hat{\boldsymbol{q}}} + \underline{\boldsymbol{\phi}}^* \tilde{\hat{\boldsymbol{q}}} + \tilde{\underline{\boldsymbol{\phi}}}^* \hat{\boldsymbol{q}}). \end{aligned} \tag{13}$$

The application of the variational principle ($\delta\mathcal{L} = 0$) to (13) yields four sets of the discretized equations of motion for the whole system; the one corresponding to the real system is given in (14) at the bottom of the page. All the notations refer to the same definition, but for the whole system this time made of simple piezoelectric material. $\boldsymbol{\phi}_1$ is the nodal potential vector induced over the electrodes due to the applied charge vector $\hat{\boldsymbol{q}}$ for excitation. Subscript 1 refers to the nodes associated with the electrodes and subscript 2 to the nodes of the region without electrodes. The mechanical loss is due to the structural damping, for which the stiffness is simply evaluated as of complex value. On the other hand, Ω/ω in (14) expresses the effect of rotation, with which the mass is now also evaluated as of complex value, and providing phase lag in the motion. The term for the rotation in the system matrix in (14) appears to cause additional damping. It should be noted, however, that the direction of the displacement which is included by Coriolis force due to rotation is orthogonal to the direction of the vibratory displacement (no diagonal term presents in the matrix of rotation), so that no dissipation takes place. The rotational effect increases as the vibratory angular frequency decreases. When the system is stationary ($\Omega = 0$), (14) arrives at the same conclusion as found in the usual finite element expression for piezoelectric vibrations. In the present case, as the matrix of rotation $\boldsymbol{\Theta}$ is nonsymmetric, the system matrix in (14) is complex and nonsymmetric. The eigenvalues are therefore complex, but when no damping is assumed to exist, the eigenvalues are real, as the system matrix is Hermitian.

IV. Numerical Examples

Equation (14) is implemented on a computer code to simulate the behavior of the piezoelectric vibrator gyroscopes. The gyroscopes considered here are made of a thin plate and have pairs of electrodes on both their faces for driving and detecting. Here, the plate made of electrostrictive ceramics is considered. The material properties of the piezoelectric ceramics (NEPEC 6, TOKIN Corp.) are given in Table I. For the calculation of the natural frequencies of the free vibration, both the LU decomposition method and determinant search method are used, and the inverse power method is also incorporated for the natural mode evaluation. For the forced responses, the LU decomposition method is used. All of the calculations are made for complex quantities with double precision.

A. A Square Thin Plate

We first consider the case of the simplest monolithic gyroscope made of a thin piezoelectric square plate. The plate provides pairs of the partial electrodes. Electrode arrangement and the finite element division are shown in Fig. 4. The plate is driven by the pairs of four electrodes distributed around its center and the electrodes for detection are placed in its four corners.

TABLE I
Material Properties of Piezoelectric Ceramics (NEPEC 6)

s^E	$\begin{bmatrix} 12.7 & -4.1 & 0.0 \\ & 12.7 & 0.0 \\ \text{sym.} & & 33.5 \end{bmatrix} \times 10^{-12}$ (m²/N)
d	$\{-133 \ -133 \ 0\} \times 10^{-12}$ (C/N)
$\varepsilon_{33}^T/\varepsilon_0$	1050
ρ	7730 (kg/m³)
Q_m	1500
$\tan\delta$	0.3 (%)

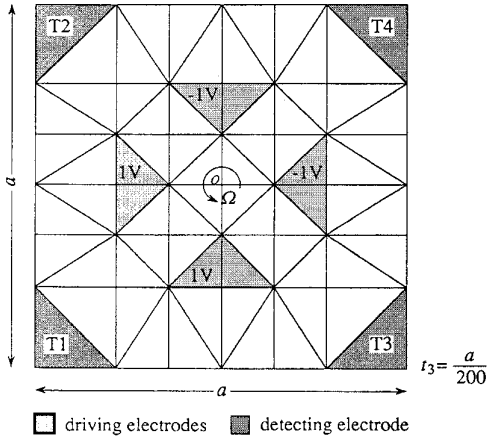

Fig. 4. Piezoelectric thin plate gyroscope–electrode arrangement and finite element division.

1) Natural Frequencies and Modes: The case in which the thin plate is simply elastic without piezoelectricity and damping is examined first. The behaviors of the piezoelectric thin plate in plane motion have been well examined [9]. To observe the effect of the rotation, the natural frequencies and modes of free vibration are compared with those in rotation. The natural modes without rotation are shown in Fig. 5, in which $\overline{f}_n$ are the natural frequencies of a square plate of $a \times a$, normalized with respect to $f_{LB}\,[= 1/(2a\sqrt{s_{11}^E\rho})]$, the natural frequency of longitudinal vibration of a thin bar of length a. The second, sixth, and eighth modes ($\overline{f}_2$, $\overline{f}_6$, $\overline{f}_8$) are degenerated modes. When the piezoelectric effect is included, the natural frequencies increase as much as a few percent, though they depend also on the condition at the electrical terminals, and

$$\left(\begin{bmatrix} \boldsymbol{K} - \omega^2\boldsymbol{M} & \boldsymbol{P}_1 & \boldsymbol{P}_2 \\ \boldsymbol{P}_1{}^* & -\boldsymbol{G}_{11} & -\boldsymbol{G}_{12} \\ \boldsymbol{P}_2{}^* & -\boldsymbol{G}_{12}{}^* & -\boldsymbol{G}_{22} \end{bmatrix} + j \begin{bmatrix} \frac{1}{Q_m}\left(\boldsymbol{K} - 2\omega^2\frac{\Omega}{\omega}Q_m\boldsymbol{\Theta}\boldsymbol{M}\right) & \boldsymbol{0} & \boldsymbol{0} \\ \boldsymbol{0} & \tan\delta\boldsymbol{G}_{11} & \tan\delta\boldsymbol{G}_{12} \\ \boldsymbol{0} & \tan\delta\boldsymbol{G}_{12}{}^* & \tan\delta\boldsymbol{G}_{22} \end{bmatrix} \right) \times \begin{bmatrix} \boldsymbol{\xi} \\ \boldsymbol{\phi}_1 \\ \boldsymbol{\phi}_2 \end{bmatrix} = \begin{bmatrix} \boldsymbol{0} \\ \hat{\boldsymbol{q}} \\ \boldsymbol{0} \end{bmatrix} \quad (14)$$

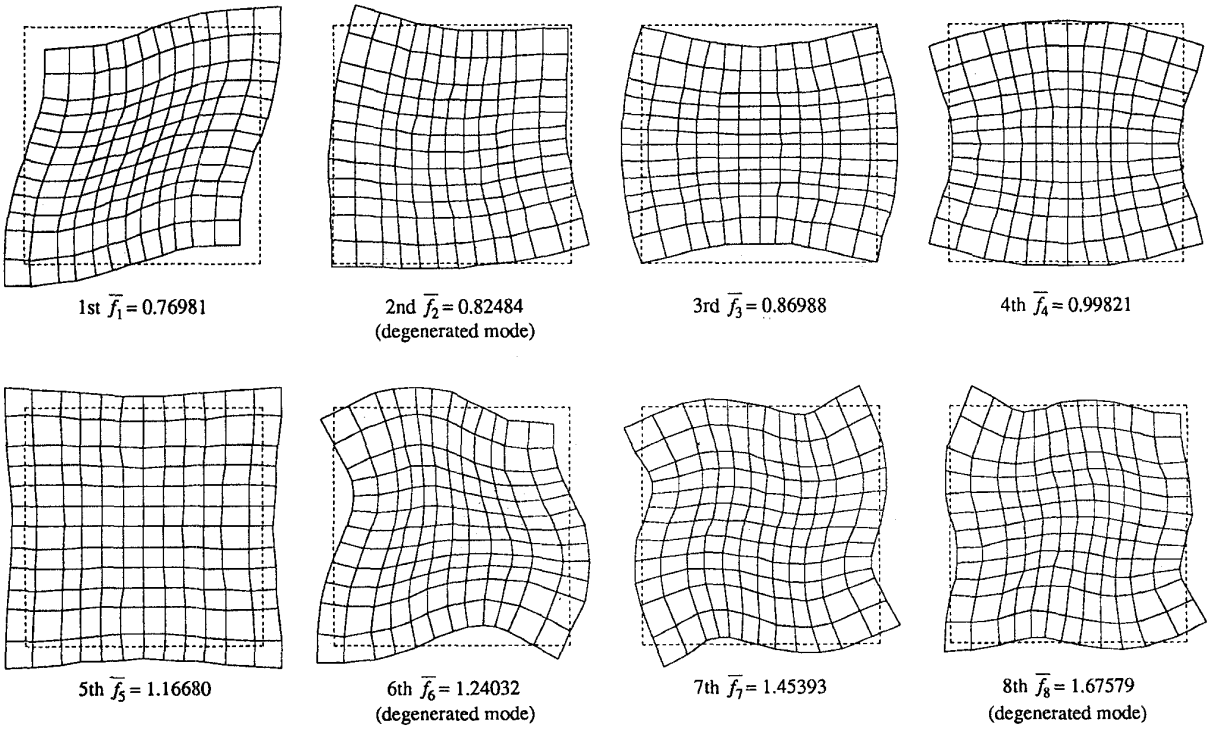

Fig. 5. Modal patterns and corresponding natural frequencies (no rotation, $\overline{f}_n$: frequency normalized with respect to f_{LB}).

the order of the natural frequencies may interchange between the second and third modes, as well as between the fifth and sixth modes. The effect of the rotation is then considered. The first and second modes are shown in Fig. 6. The normalized rotational angular frequency $\overline{\Omega}(= \Omega/2\pi f_{LB})$ is chosen to be 6.3×10^{-4}. The modes become complex in rotation as expected, and it should be noted that degeneration is resolved for the second mode (degenerated without rotation) which separates into two modes, the lower mode $(\overline{f}_{2L})$ and upper mode $(\overline{f}_{2U})$. This also occurs for the other degenerated modes. The separation of the degenerated modes is caused due to the appearance of the mass anisotropy in the plate because the Coriolis force is perpendicular to the direction of the inertia force (see the matrix of rotation $\boldsymbol{\Theta}$ in the Nomenclature). The modal shapes of the imaginary part are the same as the ones of the real part except that they are only rotated clockwise or anticlockwise by 90°. Fig. 7 shows the change of the normalized natural frequencies of the second modes against the normalized rotational angular frequency. The natural frequencies increase or decrease in proportion to the rotational angular frequency for $\overline{\Omega} \ll 1$. The change of the natural frequencies may occur for other nondegenerated modes when the plate rotates, but the rate of the change of their natural frequencies is very small.

2) Gyroscopic Characteristic: The square plate gyroscope is then considered, in which both mechanical and dielectric damping properties are included $(1/Q_m = 6.67 \times 10^{-4}$, $\tan\delta = 0.3\%)$. When pairs of the four electrodes placed around the center of the plate are driven by a voltage of ± 1 V at frequency $\overline{f}$ as shown in Fig. 4, the driving electrical input admittance characteristic at a pair of the electrodes near the second mode resonant frequency is shown in Fig. 8. The input admittance is normalized with respect to the admittance of damped capacitance at frequency f_{LB}. As the electrodes are arranged symmetrically, it is the same for each pair of driving electrodes. And, to observe the effect of rotation, the open–circuit voltage that appears in the detecting electrodes provided at the corners is shown in Fig. 9. Fig. 9(a) shows the change of the output voltage in Terminal 1 (T1) and Fig. 9(b) shows the voltage in Terminal 2 (T2). For both cases the output is complex indicating the phase shift in the transmission. Solid lines are the cases without rotation and the broken lines are the cases with rotation of $\overline{\Omega} = 6.3 \times 10^{-4}$. In T1, the voltage appears in the vicinity of the resonant frequency which, however, is not much effected by rotation. In T2, the voltage appears only when the rotation takes place. This makes it possible to detect the rotation. The output voltages in T3 and T4 are the same as the voltage in T2 and T1, except the sign is reversed. The sign of the output voltages is also reversed for the rotation reversed. Fig. 10 shows the change of output voltage against the normalized rotational angular frequency $\overline{\Omega}$ for the input voltage of one volt on the driving electrodes given. As expected from Fig. 9, only the output voltages in T2 and T3 are sensitive to the rotation, and their changes are proportional to the rotational angular frequency. We define here the normalized figure of merit η as

$$\eta = \frac{1}{2}\frac{V_o}{V_i}\frac{1}{Q_m}\frac{1}{\overline{\Omega}} \tag{15}$$

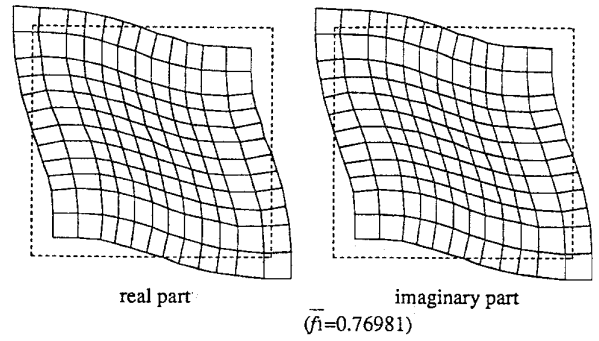

Fig. 6. Modal patterns of the plate in rotation ($\bar{\Omega} = \Omega/\omega_{LB} = 6.3\times10^{-4}$), (a) first and (b) second modes. No damping is included.

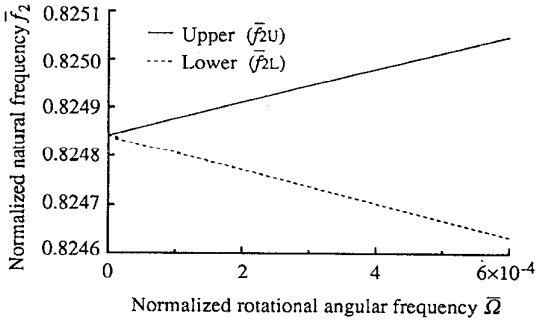

Fig. 7. Change or separation of the natural frequency as the increase of rotation.

where V_i and V_o are input and output voltage, respectively. The normalized figure of merit η of the present square plate

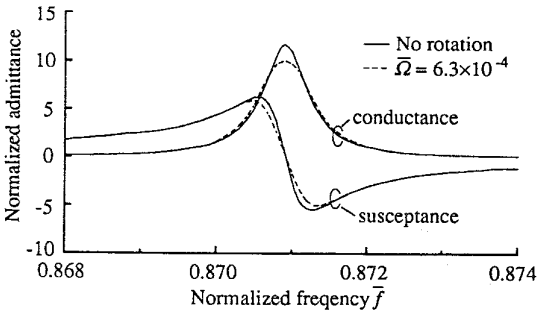

Fig. 8. Effect of the rotation on the input admittance at the electrical terminals, second mode. Both mechanical and dielectric losses are included.

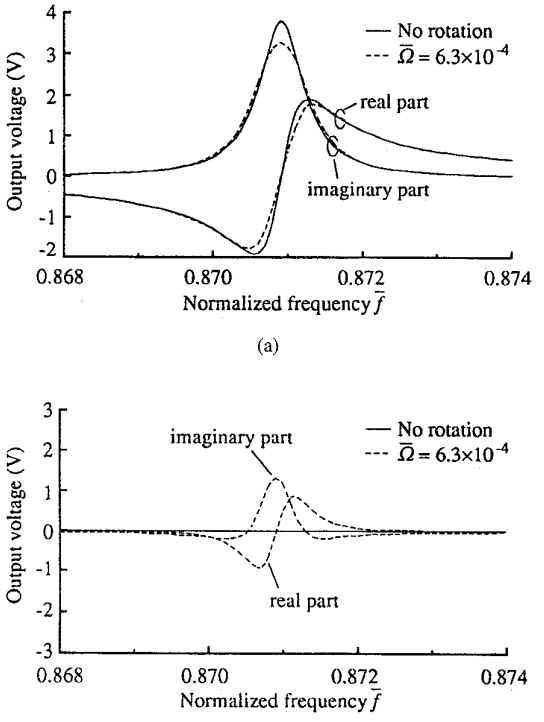

Fig. 9. Effect of the rotation on the output voltage, second mode, (a) at T1 and (b) at T2.

is 0.82, which is not satisfactory for practical applications, though the sensitivity could be doubled with the differential connection of the electrodes in T2 and T3. This differential operation could be used to establish the temperature stability, as the effect of the temperature on the change of the natural frequency must be the same for each terminal.

B. Cross-Bar Gyroscope

Equation (14) suggests that the natural frequency must be chosen as low as possible for realizing the high sensitivity. Here, we employ flexural modes in plane. The configuration made of crossed bars shown in Fig. 11 is a candidate in which two bars are coupled at their center, supported at some places. This could be made of a piezoelectric thin plate with the etching process removing the shaded portions. In the present

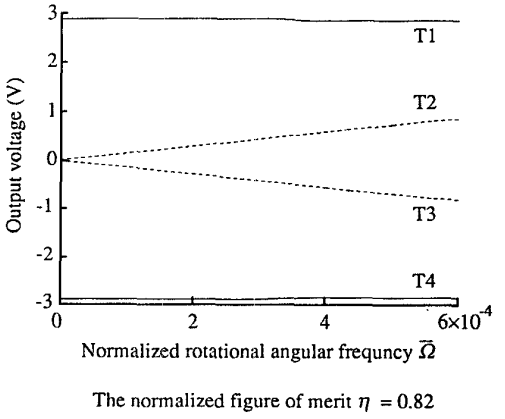

Fig. 10. Change of the output voltage against the rotation (input: 1 V).

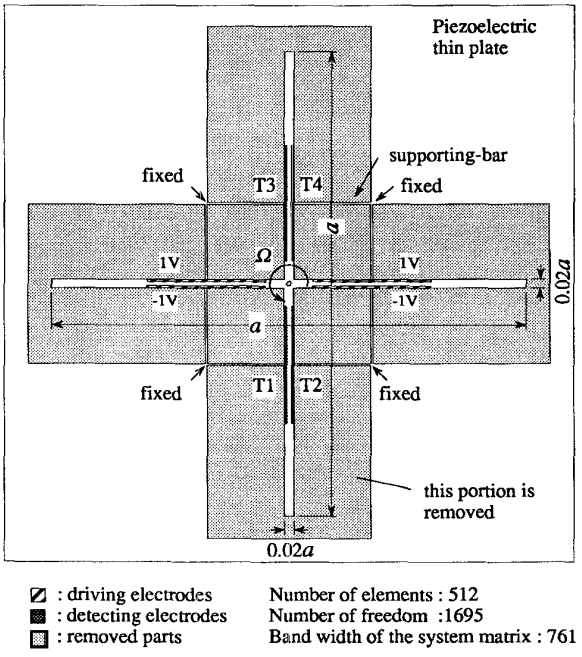

Fig. 11. Cross-bar gyroscope.

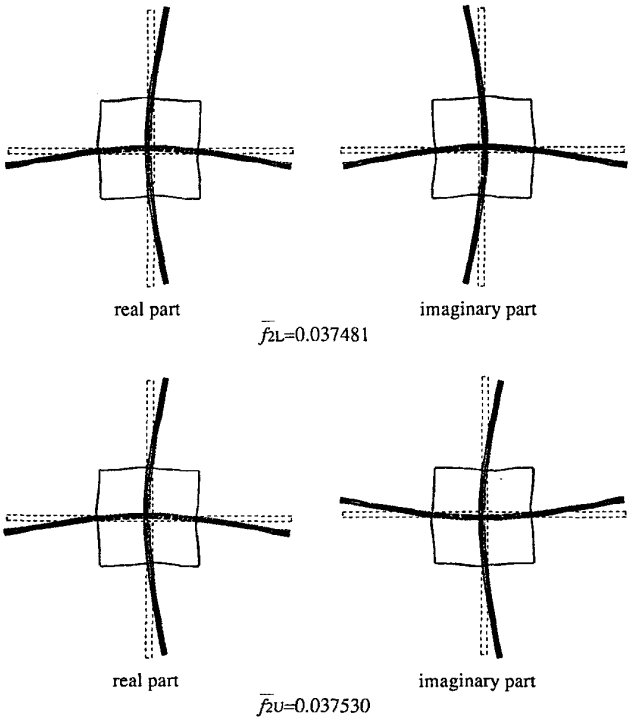

Fig. 12. Modes of cross-bar gyroscope in rotation ($\overline{\Omega} = \Omega/\omega_{LB} = 6.3 \times 10^{-5}$, loss is neglected).

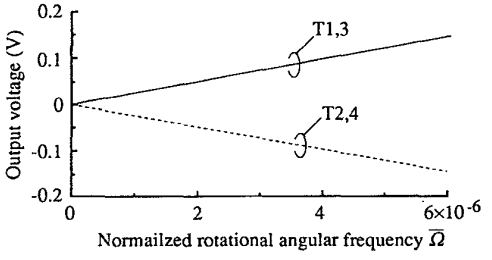

Fig. 13. Change of the output voltage against the rotation (input: 1 V).

model, only the crossed bars including supporting bars which are fixed at the other ends are considered for the analysis. NEPEC 6 is again assumed for the piezoelectric thin plate.

The natural modes of vibration are shown in Fig. 12 for the lowest degenerated modes in rotation ($\overline{\Omega} = 6.3 \times 10^{-5}$). Piezoelectric effect is included, but not damping. The modes are complex in which degeneration is resolved, so that the mode separates into two modes ($\overline{f}_{2L}$, $\overline{f}_{2U}$). Fig. 13 shows the change of the open-circuit output voltage against the normalized rotational angular frequency $\overline{\Omega}$ for the input voltage of one volt on the driving electrodes. In this calculation, both dampings of the material are included. The output voltage is equal in T1 and T3, and also in T2 and T4. The normalized figure of merit η is 8.1. The sensitivity or figure of merit is now improved as much as about ten times compared with that of the square plate gyroscope.

C. Ring-Plate Gyroscope

The vibrator gyroscope first developed was the one making use of the bending modes associated with a bell-shaped configuration. This is a plate version of the original configuration made of a piezoelectric thin plate which is shown in Fig. 14. A ring-plate is partly supported with the shaded portions removed. Only the ring including the supporting bars is considered for the analysis, and NEPEC 6 is again assumed for the material.

1) Ring-Plate Without Support: We first consider the case without supporting bars. The finite element division and the electrode arrangement are shown in Fig. 15. The natural modes of vibration are shown in Fig. 16 for the second modes in rotation ($\overline{\Omega} = 6.3 \times 10^{-6}$), which include the piezoelectric effect and the electrodes but not damping. The modes are originally degenerated without rotation. The modes separating

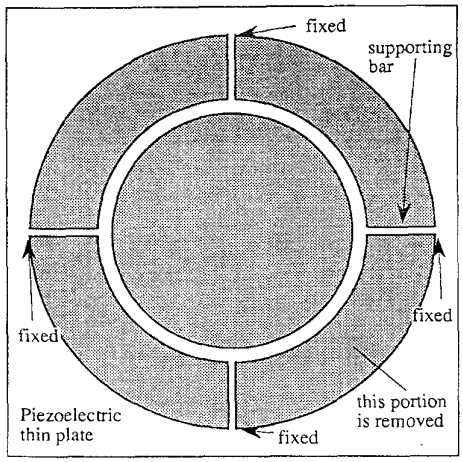

Fig. 14. Ring-plate type gyroscope.

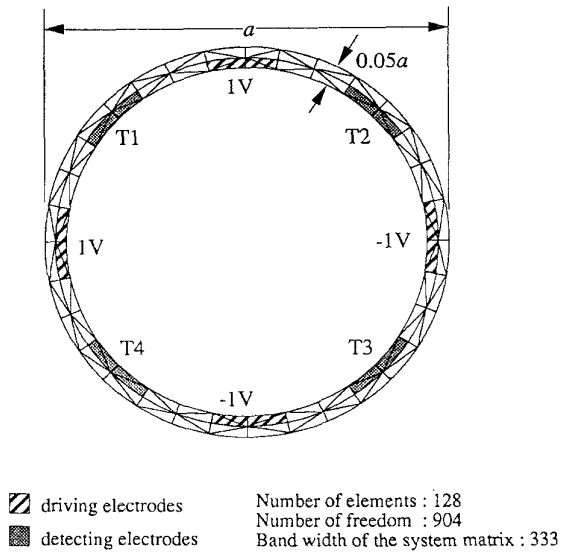

Fig. 15. Ring-plate piezoelectric vibrator gyroscope, electrode arrangement, and finite element division.

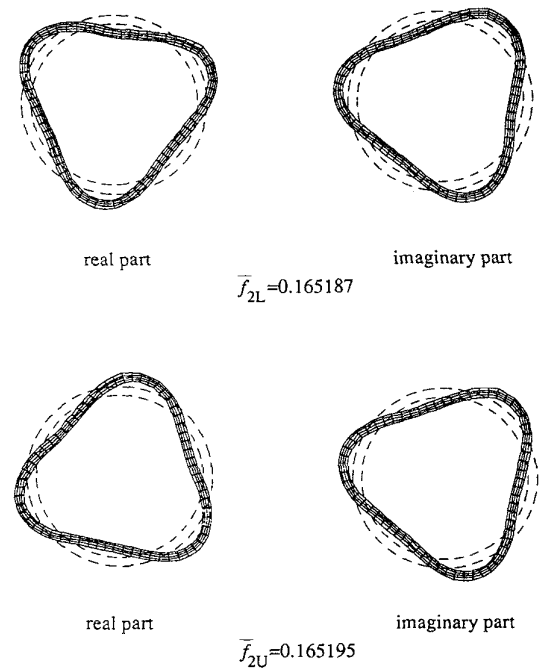

Fig. 16. Second modes of ring-plate gyroscope in rotation ($\overline{\Omega} = \Omega/\omega_{LB} = 6.3 \times 10^{-6}$, loss is neglected), without support.

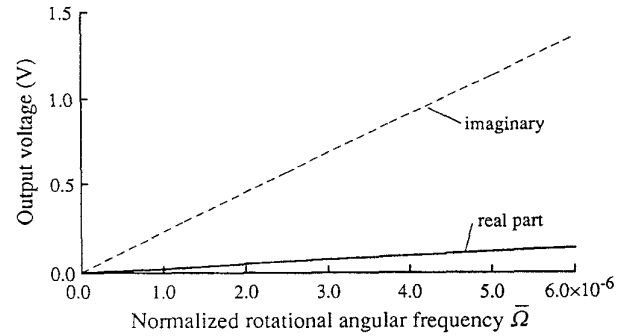

The normalized figure of merit η = 75.4

Fig. 17. Change of the output voltage against rotation at T4 (input voltage: 1 V), without supporting bars.

into two modes ($\overline{f}_{2L}$, $\overline{f}_{2U}$) are complex due to the effect of the rotation as the degeneration is resolved.

Fig. 17 shows the change of the open-circuit output voltage against the normalized rotational angular frequency $\overline{\Omega}$ for the input voltage of one volt on the driving electrodes. The dampings are included. The output voltages are equal in T2 and T4 in the amplitude, but reversed in phase. The phase shift is observed, as the driving frequency does not completely meet the resonant frequency in the present case. (The output voltages are not sensitive against rotation both in T1 and T3.) The normalized figure of merit η is 75.4. The sensitivity is now improved as much as 9.3 times compared with that of the cross-bar gyroscope.

2) Ring-Plate with Support: We next consider the case when the supporting system is included. The element division and the electrode arrangement is shown in Fig. 18. Supporting bars are added to the ring-plate. The natural modes of vibration are shown in Fig. 19 for the second modes in rotation ($\overline{\Omega} = 6.3 \times 10^{-6}$) for the width $w = 2.56 \times 10^{-4} a$. Like the ring-plate without support, the modes are again complex separating into two modes ($\overline{f}_{3L}$, $\overline{f}_{3U}$), which correspond to the second modes of the ring-plate without support. The modal shapes are not much affected by the presence of the supporting bars which are very thin.

Fig. 20 shows the change of the open-circuit output voltage against the normalized rotational angular frequency $\overline{\Omega}$ for the input voltage of one volt on the driving electrodes. The dampings are included. The output voltages are equal in T2 and T4 in amplitude, but reversed in phase. The output voltage is not sensitive to rotation both in T1 and T3. The normalized figure of merit η is 60.5. The sensitivity is slightly decreased compared with the case without support.

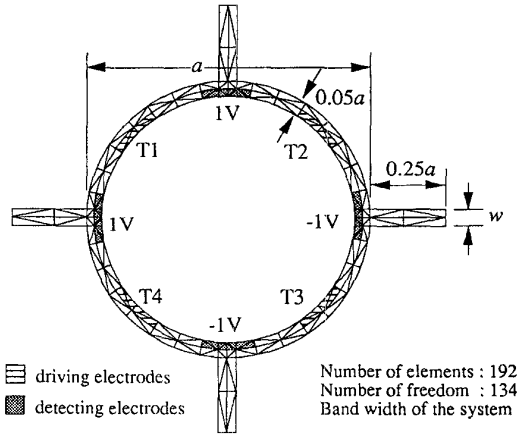

Fig. 18. Finite element division and electrode arrangement when the supporting bars are included.

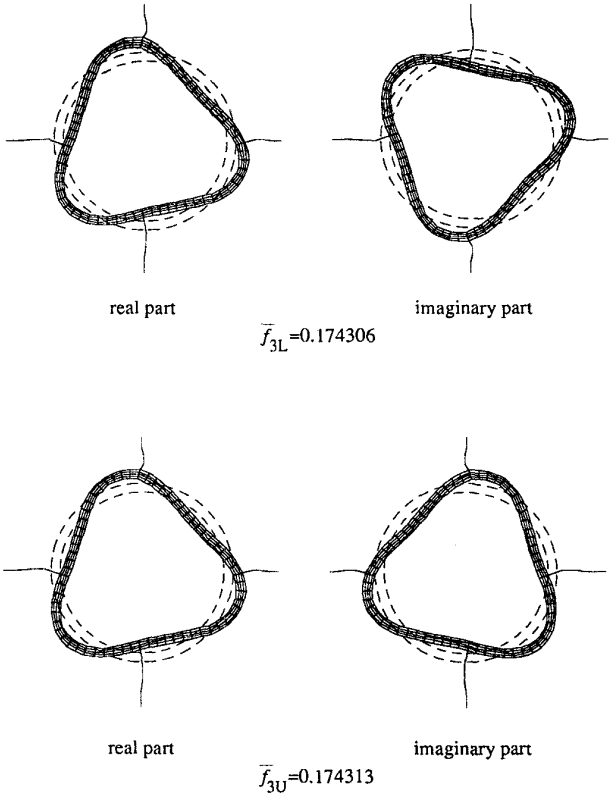

Fig. 19. Second modes of ring-plate gyroscope in rotation ($\bar{\Omega} = \Omega/\omega_{LB} = 6.3 \times 10^{-6}$, loss is neglected), with support.

The effects of the rigidity of the supporting bars on the resonant frequency of the third modes are shown in Fig. 21, in which the frequency deviation against the width of the supporting bars is given.

For these particular modes of vibration, the electrodes and the supporting bars may not be best placed for sensing the rotation. This can be achieved through simulation procedures. The numerical examples are shown only for the purpose of demonstration.

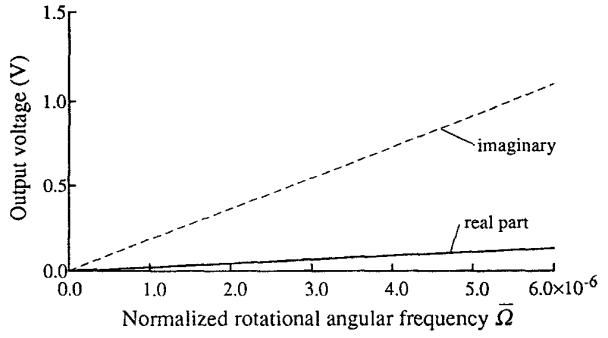

The normalized figure of merit $\eta = 60.5$

Fig. 20. Change of the output voltage against rotation bars at T4 (input voltage: 1 V), with support.

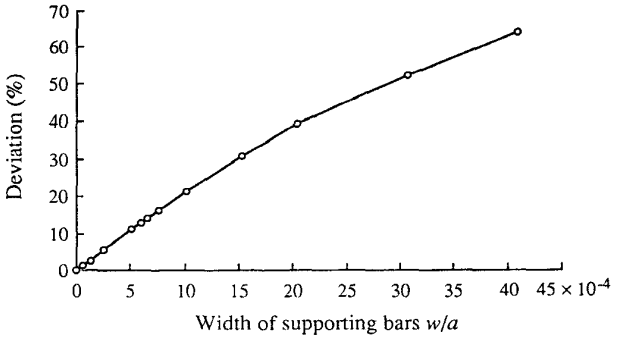

Fig. 21. Deviation of resonant frequency against the width of supporting bars referring to resonant frequency without support.

V. Concluding Remarks

The use of the finite element approach is proposed for the characteristic prediction of piezoelectric vibrator gyroscopes. The finite element formulation including the effect of Coriolis force due to rotation is given for a piezoelectric thin plate in plane vibration, which is considered as a two-dimensional model.

Using the computer program developed, the modal shapes, electric input admittance, the change of the transmission characteristic, or the output voltage due to the rotation are demonstrated for three types of vibrators where the development of the gyroscopes of monolithic configuration is kept in mind.

The following could be deduced from the examination:

1) The property of Coriolis force is clearly represented in the finite element formulation, which shows that the vibratory frequency must be chosen as low as possible for high sensitivity to rotation. The sensitivity also depends on the quality factor of the modes.
2) When flexural modes are used in low frequency range, out-of-plane motion may be involved. In this case, the assumption of the in-plane vibration may fall, so that three-dimensional analysis [10] will be required.
3) The simulation shows that the two types of monolithic configuration, cross-bar and ring-plate, making use of the flexural vibration in plane, can be promising for sensitive sensing of the rotation.

4) The degenerated modes separate into two modes, the upper and the lower, due to the rotation. These modes can be advantageously utilized to provide the temperature stability, as the effect of the temperature change is the same on the resolved natural frequencies, which could be canceled. The temperature characteristic is an important factor for the device design, which can be easily incorporated into the program [11]. The inclusion of the temperature characteristic for a crystal quartz plate is now under way, which will be reported in due course of time.

The next step of this research should include the temperature effects.

REFERENCES

[1] W. D. Gates, "Vibrating angular rate sensor may threaten the gyroscope," *Electron.,* vol. 10, pp. 130–134, 1968.

[2] M. Konno, S. Sugawara, S. Oyama, and H. Nakamura, "Equivalent circuit for piezoelectric vibratory gyro of angular rate sensor," *Trans. Inst. Electron., Inform. Commun. Eng.,* vol. J70-A, no. 11, pp. 1724–1727, 1987 (in Japanese).

[3] C. S. Chou, J. W. Yang, Y. C. Hwang, and H. J. Yang, "Analysis on vibrating piezoelectric beam gyroscope," *Int. J. Appl. Electromagn. Materials,* vol. 2, no. 3, pp. 227–241, 1991.

[4] Y. Kagawa and G. M. L. Gladwell, "Application of a finite element method to vibration problems in which electrical and mechanical systems are coupled—An analysis of flexure-type vibrators with electrostrictive transducers," *IEEE Trans. Sonics Ultrason.,* vol. SU-17, no. 1, 1970.

[5] Underwater Acoustics Group, "Finite elements applied to sonar transducers," in *Proc. Inst. Acoust.,* Univ. of Birmingham, England, vol. 10, no. 9, Dec. 4, 1988.

[6] Y.-K. Yong, "Fundamentals of the finite element method of a piezoelectric resonators," in *Course 6 Short Tutorial Course IEEE Int. Ultrason. Symp.,* Cannes, France, 1994.

[7] G. M. Reese, E. L. Marek, and D. W. Lobitz, "Three dimensional finite element calculations of an experimental quartz rotation sensor," in *IEEE Ultrason. Symp.,* 1989, pp. 419–422.

[8] G. M. L. Gladwell, "A variational formulation of damped acousto-structural vibration problems," *J. Sound Vib.,* vol. 4, no. 2, pp. 172–186, 1966.

[9] Y. Kagawa and T. Yamabuchi, "Finite element simulation of two-dimensional electromechanical resonators," *IEEE Trans. Sonics Ultrason.,* vol. SU-21, no. 4, pp. 275–283, 1974.

[10] Y. Kagawa, T. Tsuchiya, and T. Kataoka, "Finite element simulation of dynamic response of piezoelectric actuators," *J. Sound Vib.,* vol. 191, no. 4, pp. 519–538, 1996.

[11] Y. Kagawa, H. Maeda, and M. Nakazawa, "Finite element approach to frequency-temperature characteristic prediction of rotated quartz crystal plate resonators," *IEEE Trans. Sonics Ultrason.,* vol. SU-28, vol. 4, pp. 257–264, 1981.

[12] Y. Kagawa, T. Tsuchiya, T. Kawashima, and E. Ando, "Finite element analysis for piezoelectric gyroscopes," Inst. Electron., Inform., Commun. Eng., Tech. Rep., vol. US93-70, pp. 47–54, Nov. 1993 (in Japanese).

Yukio Kagawa (SM'75–F'86) received the B.Eng., M.Eng., and D.Eng. degrees in 1958, 1960, and 1963, respectively, all from Tohoku University, Japan.

In 1970, he was appointed Professor of Electrical Engineering, Toyama University, Japan. Currently, he is a Professor of Electrical and Electronic Engineering, Okayama University, Japan, and Professor Emeritus, Toyama University. His present interests include the application of the numerical approach to the simulation of acoustic and electromagnetic fields and systems, especially inverse problems.

Dr. Kagawa is a fellow of the Institute of Acoustics (U.K.) and appears in *Who's Who in the World.*

Takao Tsuchiya received the B.Eng., M.Eng., and D.Eng. degrees in 1984, 1986, and 1989, respectively, all from Doshisha University, Japan.

From 1989 to 1990, he was with the Department of Electrical and Information Engineering, Toyama University, Japan. Since 1990, he has been with the Department of Electrical and Electronic Engineering, Okayama University, Japan, and he is currently a Lecturer working mainly on the numerical simulation of acoustic problems.

Toshikazu Kawashima received the B.Eng. and M.Eng. degrees in 1993 and 1995, respectively, both from Okayama University, Japan.

Since 1995, he has been with Matsushita Electric Works Co., Limited.